CHAPTER 5

GROWTH OF SILICON NANOWIRES USING INDIUM CATALYST BY HOT-WIRE CHEMICAL VAPOUR DEPOSITION

5.1 INTRODUCTION

The results and discussion in chapter 4 showed that In can act as an alternative effective catalyst to induce the growth of SiNWs. In has a low melting point of 156.6^{o}C, while molten In droplets are suitable for VLS growth process in catalytic growth of NWs, Thus making it a promising catalyst for low temperature growth of SiNWs. The low diffusivity of In into Si ($\sim 1 \times 10^{-15}$ cm^{2}/s at 900^{o}C (*Suzuki et al. 1999*)) is another promising factor regarding the production of high purity SiNWs.

The utilization of higher rf power in hot-wire assisted PECVD growth of SiNWs has been shown to increase the number density of the NWs in the previous chapter. Nevertheless, the undesired ion bombardment effect created by the plasma dissociated ionic species can be detrimental to the crystalline structures in the SiNWs (*Adachi et al. 2010; Hofmann et al. 2003*). The HWCVD technique has the advantage of an ion free deposition and effectively high SiH_4 gas dissociation through thermal heating of filament coils at temperatures of 1500^{o}C and above (*Tonokura et al. 2002; Zheng and Gallagher 2006*).

In this chapter, the growth of SiNWs from In catalyst using HWCVD is studied. Hot filament made by coiled tungsten wire was utilized to evaporate In wire placed on it in H_2 plasma environment to form catalyst islands and also to decompose SiH_4 and H_2 gas for the growth of SiNWs. The detailed catalyst formation and SiNWs growth process were described in Chapter 3, Sections 3.3.4 (set 3 – 5). The important parameters, which may strongly influence the growth and structural properties of SiNWs, namely In catalyst size, filament temperature and deposition time were studied in sequential order to understand the growth mechanism of In-catalyzed SiNWs by HWCVD.

5.2 EFFECT OF INDIUM CATALYST SIZES ON FORMATION OF SILICON NANOWIRES

5.2.1 Formation of In catalyst and Si nanowires

5.2.1 a) Morphology

Figures 5.1 (a), (b) and (c) show the FESEM images of the In droplets evaporated from different lengths of In wires, l_{In} = 3, 1 and 0.5 mm, respectively. Decrease in l_{In} significantly reduces the diameter and increases the density of the In droplets. The average diameters of the In droplets are 271 ± 67, 137 ± 33 and 67 ± 17 nm for l_{In} = 3, 1 and 0.5 mm respectively. The density of the In droplets, ρ_{In} increases from 5.6 μm^{-2} to 17.3 μm^{-2} and further to 35.2 μm^{-2} for l_{In} = 3, 1 and 0.5 mm respectively. Evaporation of In wire within the H_2 plasma condition induces the formation of a cone-like structure of the In droplets. One possible reasons for the formation of this cone-like structure is proposed here. The positively charged power electrode and the grounded substrate result in the delocalization of electrons to the top side of the In droplets, thus inducing the formation of the conical structure. The tips are sharper for the smaller size In droplets.

The In droplets mentioned in Figures 5.1 (a), (b) and (c) are the catalysts used to induce the growth of the respective SiNWs shown in Figures 5.1 (d), (e) and (f). SiNWs capped with large In droplets are formed when In droplets evaporated from wire of l_{In} = 3 mm are used as catalyst. Most of the NWs grow in a random direction and possess worm-like structures with tapering diameter decreasing from the base to the top of the NWs. Better alignment of SiNWs is observed when NWs are formed from smaller In catalyst droplets produced from In wire of l_{In} = 1 mm and below.

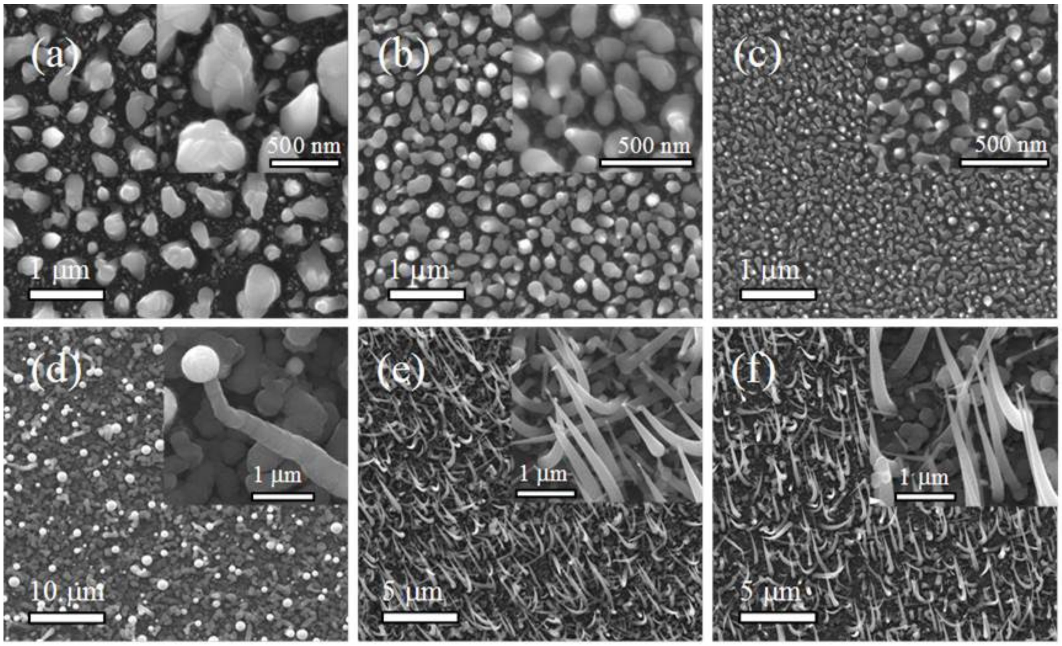

Figure 5.1: FESEM images of the In droplets evaporated from different lengths of In wires, l_{In} of (a) 3 mm, (b) 1 mm and (c) 0.5 mm, while (d), (e) and (f) are the images of the SiNWs synthesized from the corresponding l_{In}, respectively. Insets show the higher magnification of the respective images.

5.2.1 b) Tapering parameter and number density

The R_{axial} of the SiNWs is estimated by using relation 2.1. The R_{axial} increases from 200 ± 75 to 228 ± 41 and 296 ± 47 nm/min for l_{In} = 3, 1 and 0.5 mm, respectively. From the above mentioned results, shorter In wire used for evaporation results in the formation of smaller size In droplets. These smaller In droplets consume smaller amount of Si atoms to saturate in In/Si alloy droplets thus taking a shorter time for Si precipitation (*Kim et al. 2008*). This explains the increase in the R_{axial} of SiNWs formed from smaller In droplets.

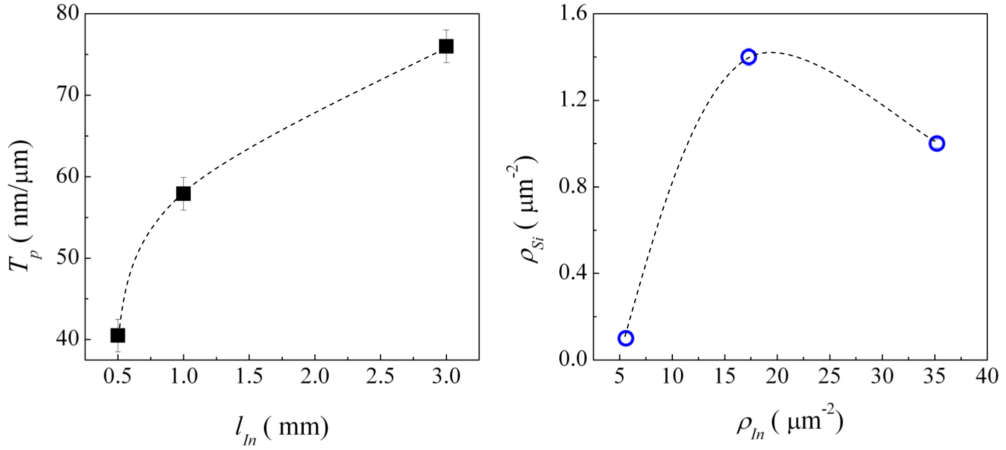

Figure 5.2: Variations of tapering parameter, T_p and number density, ρ of SiNWs with l_{In}.

The NWs tapering is mainly due to the radial growth (*Sharma et al. 2004*). As the NWs elongate from the In droplets, the base of the NWs remains exposed to the reactive radicals for longer than the NWs that are grown subsequently. This caused a gradual decrease in the diameter of the NWs from the base to the top of the NWs. The tapering parameter, T_p, of the NWs is defined as (*Joyce et al. 2009*):

$$T_p = \frac{R_{radial}}{R_{axial}} \tag{5.1}$$

where R_{radial} is the radial growth rate, which is calculated from the difference in radius of NWs, Δr_{NW} as:

$$\Delta r_{\mathrm{NW}} = r_{\mathrm{base}} - r_{\mathrm{top}} \tag{5.2}$$

per unit t_{d}. The variation of T_p with l_{In} is illustrated in Figure 5.2 (a). The calculated T_p decreases from 76 nm/μm to 57.9 nm/μm and further down to 40.5 nm/μm for l_{In} = 3, 1 and 0.5 mm, respectively. This shows that smaller size In droplets leads to less tapering in the NWs. This can be correlated to the higher R_{axial} for smaller In droplets catalyzing SiNWs as discussed in the previous paragraph.

The number densities of SiNWs per unit area, ρ_{Si} measured from FESEM images however do not show consistently increasing trend with increasing density of In droplets. From Figure 5.2 (b), ρ_{Si} increases from 0.1 to 1.4 μm^{-2} when the ρ_{In} increases from 5.6 μm^{-2} to 17.3 μm^{-2} but decreases to 1.0 μm^{-2} for the ρ_{In} = 35.2 μm^{-2}. The highest In droplets density distribution does not yield the highest density distribution of NWs. Similar results were reported by Sharma et al. (*Sharma et al. 2005a*) when optimizing the size of the Au layer to grow SiNWs in CVD. This indicates that there is a minimum size limit for the In droplets to effectively induce the growth of SiNWs. The SiH_3 radicals diffusing into molten In droplets can either homogeneously form Si nuclei within the droplets, or be accumulated at the interface between In and Si substrate to precipitate. The size of the Si nuclei is generally dependent on the temperature and deposition rate of the SiH_3 radicals. For smaller size of In droplets, the relative size of the Si nuclei to the droplets becomes larger. Moreover, molten In droplets reveal a large contact angle (~125 ^{o}) with Si substrate at temperature of 400^{o}C (*Mattila et al. 2006*). The Si nuclei could cover the interface of In and Si substrate, so that the continuous feeding of Si adatoms can only increase the size of the Si nuclei rather than precipitate to form NWs. Hence, the possibility of the SiNWs formation from the In droplet with a size below the minimum size limit is strongly restricted. One of the possibilities to solve this problem is to control the temperature or deposition rate of the SiH_4 gas precursor.

5.2.2 Energy dispersive X-ray spectroscopy

The EDX spectra scanned on the In-catalyzed SiNWs are presented in Figure 5.3. The EDX scanned on the catalyst cap [EDX spectrum 1] shows significant presence of Si with wt% of 76.86% compared to the presence of trace In (9.08%) and O (14.06%) contents. The EDX spectrum 2 shows that only Si and O elements are present in the NWs with wt% of 92.85 and 7.15%, respectively. The presence of In only in the catalyst cap and not in the NWs stem shows that the NWs growth is induced by In catalyst. The high signal of Si element in the cap is contributed by the Si substrate as the penetration depth of EDX is > 1 µm. Therefore, the catalyst cap mainly consists of In and O elements. The O elements observed in both EDX spectra are contributed by a post-deposited oxide layer formed on the surface of the NWs. Due to the detection limit of the EDX, no trace of other elements with > 1 wt% was found in the EDX spectra. This indicates the SiNWs formed are at high purity.

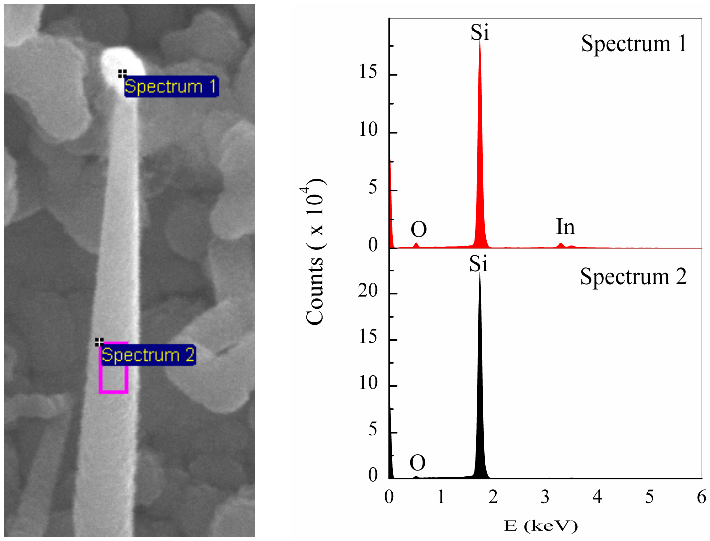

Figure 5.3: (Left hand side) FESEM image of single In-catalyzed SiNWs. (Right hand side) EDX spectra taken on the catalyst droplet (Spectrum 1) and NW stem (Spectrum 2).

5.2.3 X-ray diffraction

The structural properties of In-catalyzed SiNWs using HWCVD were studied by XRD patterns as shown in Figure 5.4. Diffraction peaks of Si and In are well indexed in the figure. The presence of strong Si diffraction peaks in all these patterns indicates the as-grown SiNWs are highly crystalline in structure. No In diffraction peak is observed in the XRD pattern for l_{In} = 0.5 mm, whereas for l_{In} = 1 mm, the In peak corresponding to (101) crystal plane is observed. The presence of In crystalline peaks due to (002), (110), (112), (103) and (211) orientations in the XRD pattern of the sample deposited using In wire of l_{In} = 3 mm indicate highers crystallinity of In droplets capping the top of these SiNWs.

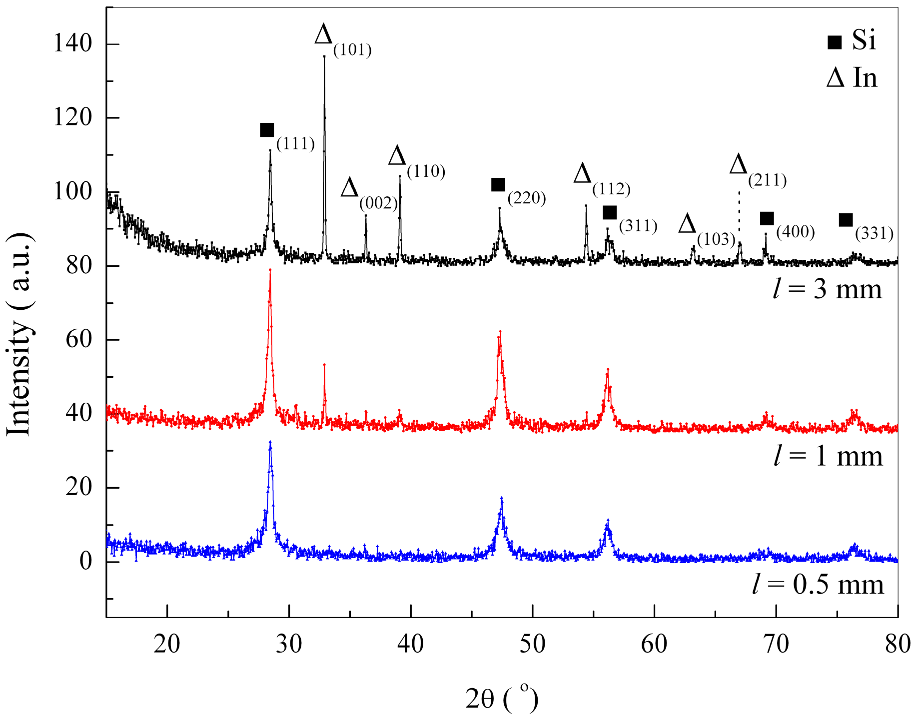

Figure 5.4: XRD patterns of the SiNWs synthesized using different lengths of In wires (l_{In} = 3, 1 and 0.5 mm). The diffraction peaks of Si and In elements are indexed to face-centered cubic Si (JCP2:00-026-1481) and body-centred tetragonal (JCP2:01-085-1409) structures, respectively.

5.2.4 Comparison of Si nanowires grown on c-Si and quartz substrates

The growth of SiNWs on p-type c-Si(111) and quartz substrates is examined by FESEM as shown in Figures 5.5 (a) and (b), respectively. These images demonstrate that similar morphology of SiNWs can be obtained via this HWCVD technique on quartz substrate. The SiNWs are more aligned in a specific growth direction on c-Si substrate, but the growth is more random in direction on quartz substrate. The XRD patterns of the In-catalyzed SiNWs prepared on both c-Si(111) and glass substrates are presented in Figure 5.5 (c). The similar X-ray characteristics of the SiNWs formed on different substrates show that the crystallinity of the NWs is not influenced by the substrates.

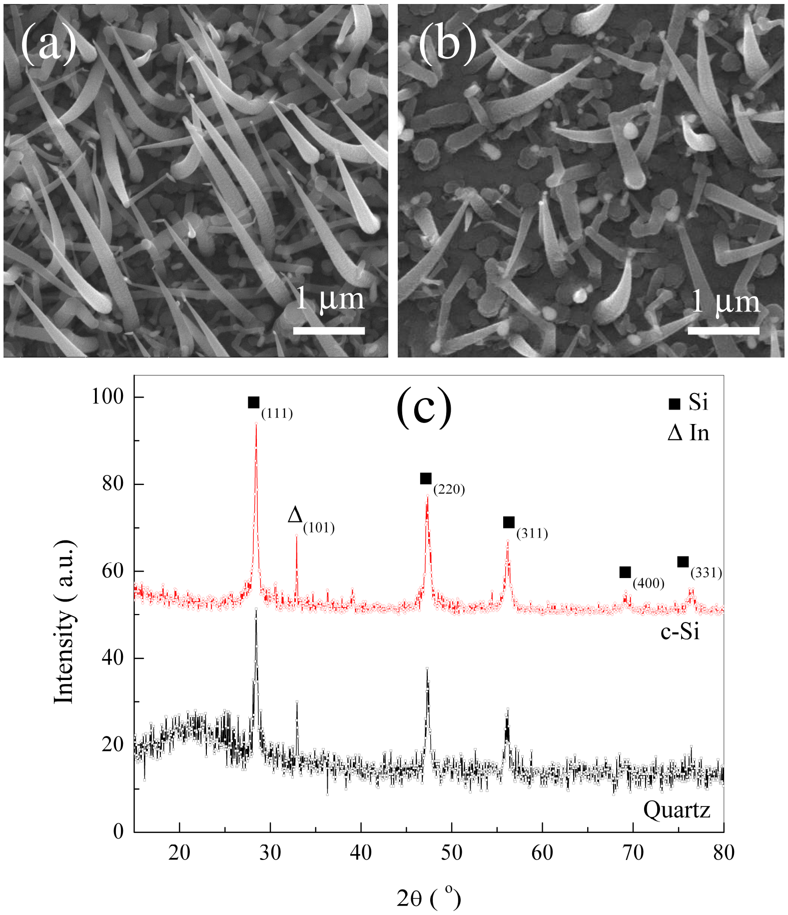

Figure 5.5: FESEM images In-catalyzed SiNWs prepared on (a) c-Si and (b) quartz substrates. (c) XRD patterns of the In-catalyzed SiNWs grown on both c-Si and quartz substrates. The crystal planes corresponding to Si and In crystal peaks were indexed according to the JCP2:00-026-1481 and JCP2:01-085-1409, respectively.

5.2.5 Growth mechanism

A simple growth mechanism proposed for growth of SiNWs induced by different In droplets sizes using HWCVD is illustrated in Figure 5.6. The largest size In droplet [Figure 5.6 (a)*i*] initially takes a cone shape due to the polarization in H_2 plasma environment as mentioned earlier, which leads to the random growth of the worm-like structure NW [Figure 5.6 (b)*i*]. During the growth, the In droplet tends to deform into a spherical shape with minimum surface energy. Decrease in size of In droplets [Figure 5.6 (a)*ii* and *iii*] induces the vertical growth of aligned and tapered NWs with small In tips on top [Figure 5.6 (b)*ii* and *iii*]. The size of In droplets is reduced during NWs growth, which indicates that the In atoms are evaporated or incorporated into the

SiNWs. However, unlike the large In droplets, the smaller sized In droplets retain their conical shape after the formation of NWs. Smaller sized In droplets induce better alignment and less tapering of NWs [Figure 5.6 (b)*iii*]. This is believed to be due to shorter nucleation time and the crystalline lattice growth.

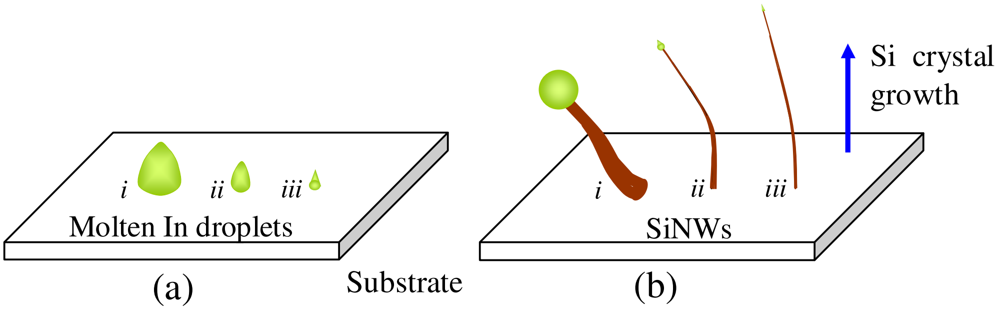

Figure 5.6: Schematic diagram of the (a) formation of different sizes of molten In droplets under H_2 plasma condition, and the (b) growth of SiNWs corresponding to molten In droplets in (a).

5.3 EFFECT OF FILAMENT TEMPERATURE ON GROWTH OF SILICON NANOWIRES

In the HWCVD process, the T_f is considered to be an important parameter since it directly affects the decomposition of the SiH_4 gas which produces different radical species for deposition. The influence of T_f on the SiH_4 decomposition has been intensively studied from both theoretical and experimental aspects in order to understand the growth mechanisms (*Duan et al. 2001; Nozaki et al. 2001; Tonokura et al. 2002; Zheng and Gallagher 2006*). The decomposition of SiH_4 and the desorption of Si and H radicals from the HW surface at a threshold T_f of ~1500°C are generally agreed upon by several reported studies (*Duan et al. 2001; Gallagher 2001; Zheng and Gallagher 2006*). For lower T_f, the release of Si radicals from the HW surface becomes negligible, as these radicals tend to be absorbed onto the surface of the filament (*Gallagher 2001*). Meanwhile, such low T_f could also cause the formation of silicides on the filament, thus resulting in incomplete decomposition of the SiH_4, producing only traces of SiH_2 and SiH_3 radicals (*Tange et al. 2001*). For T_f > 1500°C, the Si and H radicals desorb rapidly in large quantities, which then react with the SiH_4 molecules to form SiH_x and Si_2H_x radicals. If unstable or intermediate species are formed, they could initiate further reactions with other radicals to form more stable radicals. The long lifetime SiH_3 radicals remain as non-reactive species even during collisions with parent molecules or other radicals. Nevertheless, the arguments on radicals-parent molecules and radicals-radicals interactions are still a subject of debate among researchers. It is established that Si, SiH_3 and Si_2H_4 are the main growth precursors involved in the growth of HWCVD Si-based materials (*Van Veenendaal and Schropp 2002*). Effect of T_f on the growth and structural properties of In-catalyzed SiNWs are investigated in the following section.

5.3.1 Growth of Si nanostructures and nanowires at different filament temperatures

5.3.1 a) Morphology

Figures 5.7 (a) – (f) show the FESEM images of the In-catalyzed SiNWs synthesized at different T_f of 1300 to 1800°C with an increment of 100°C. At low T_f of 1300 and 1400°C, only worm-like structures and conical-shaped particles are distributed throughout the sample image. The worm-like structures are short (length ~200 – 400 nm) and randomly dispersed around the conical particles. At T_f of 1500°C, whisker-like NWs start to grow in some of the parts of the sample. This indicates that the threshold T_f lies between 1400 and 1500°C for the successive growth of the NWs. The length and diameter of the whisker-like NWs are typically ~1 μm and ~80 nm. A higher density of tapered NWs is found only in the samples grown at T_f of 1600°C and above. However, most of the NWs grown at T_f of 1600°C showed a kinked structure. The kinks in the NWs are much reduced when the T_f is increased to 1700°C and above.

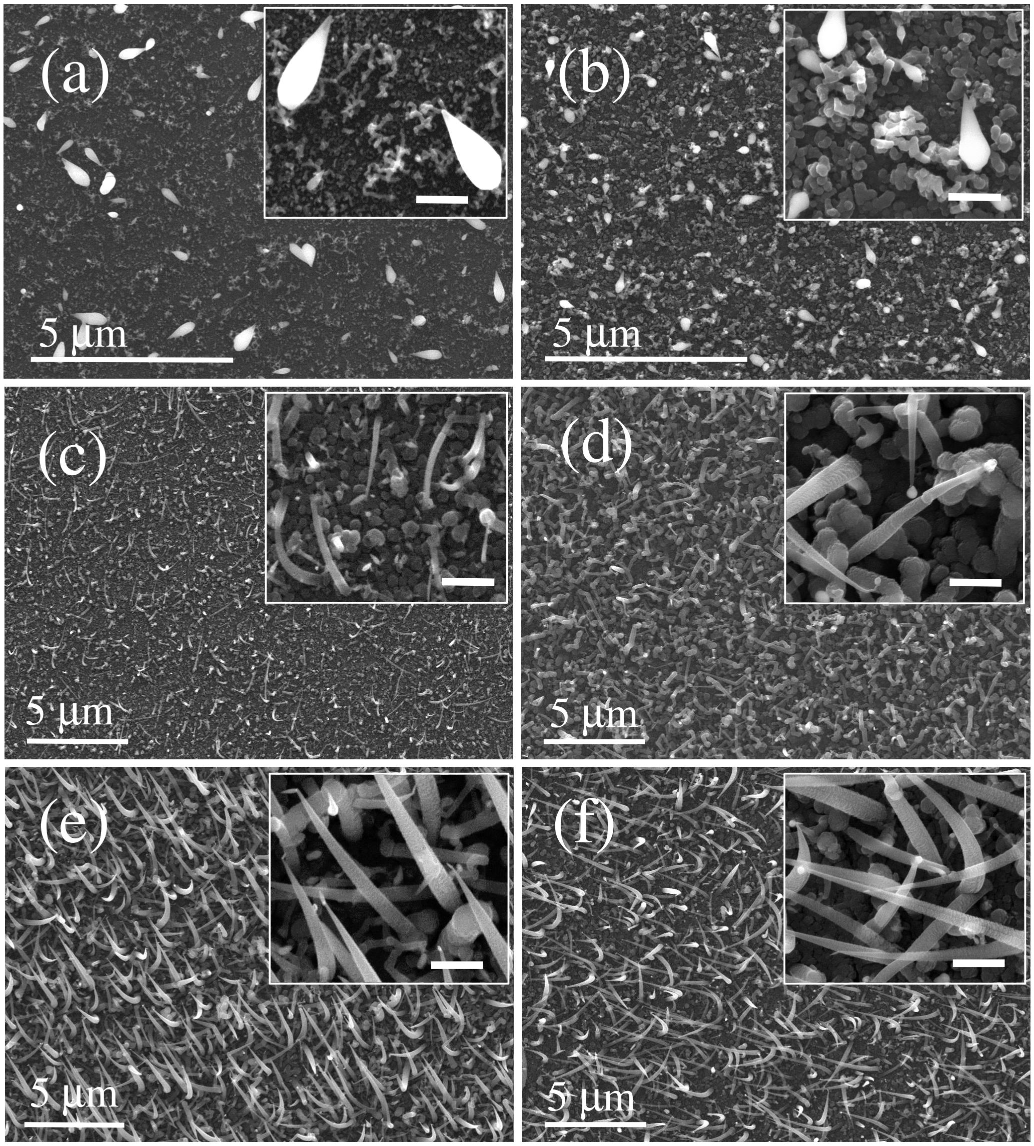

Figure 5.7: (a)-(f) FESEM images of the SiNWs samples synthesized at different T_f of 1300 to 1800°C with an increment of 100°C. Inset is the magnified features from the respective images. (Scale bar of inset= 500 nm)

5.3.1 b) Variation of number density and aspect ratio with filament temperature

The number density, ρ_{Si} and aspect ratio of the NWs grown at different T_f are illustrated in Figure 5.8. Generally, both the values of ρ_{Si} and the aspect ratio of the NWs increase with an increase in T_f. The ρ_{Si} value of the NWs reaches a maximum (1.4 ± 0.1 µm^{-2}) at T_f of 1700°C and then decrease slightly to 1.2 ± 0.1 µm^{-2} with increase in T_f to 1800°C. Meanwhile, an abrupt increase in aspect ratio of NWs from 6 ± 1 to 10 ± 2 was observed when T_f increased from 1400 to 1500°C. This was followed by an almost constant increase in aspect ratio from 10 ± 2 to 18 ± 2 when T_f was increased from 1500 to 1800°C.

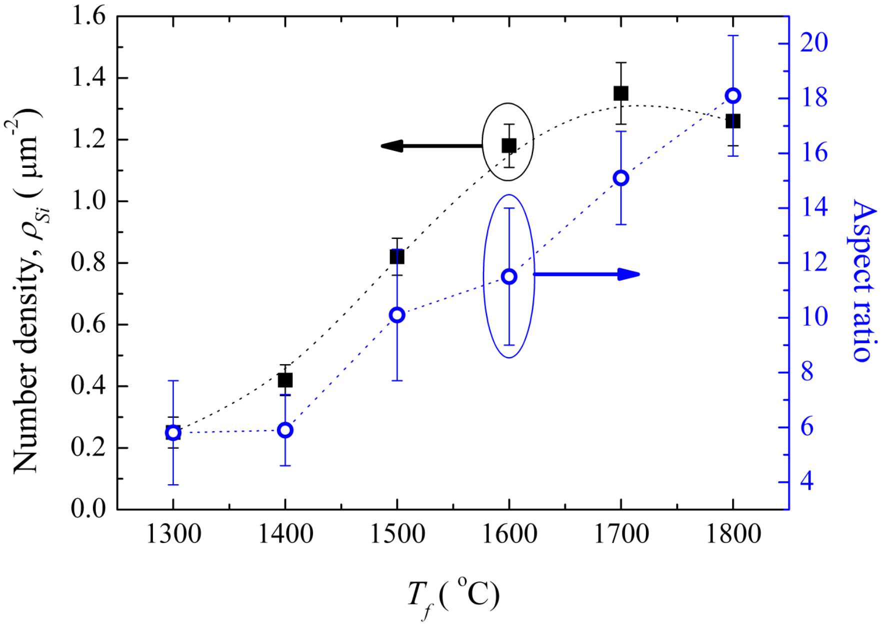

Figure 5.8: The variation number density, ρ_{Si} and aspect ratio of SiNWs with T_f.

5.3.1 c) Variation of growth rate with filament temperature

The dissociation of SiH_4 into atomic Si and H radicals begins at T_f ~1500°C. The desorbed Si atoms presumably play an important role in the success growth of SiNWs and also in inducing the secondary reactions with the parent SiH_4 molecules. This tends to generate large quantities of precursors for the growth of SiNWs. Since the SiH_4 decomposition and Si atom desorption rates are still rather low at T_f of 1500°C, it is only able to induce the growth of whisker-like SiNWs. Further increase in T_f increases the growth rate of the SiNWs. The R_{axial} is dependent on the T_f due to the decomposition probability of the SiH_4 gas. The increase in T_f at $\geq$ 1500°C has the effect of exponentially increasing the decomposition probability of SiH_4 (*Zheng and Gallagher 2006*), and the impingement rate of the Si flux on the substrate (*Klein et al. 2005*). As a result, number of precursors reaching the NWs growth sites is also greater than before. This produces SiNWs with higher R_{axial}. Here, under a constant SiH_4 flow rate and pressure, the NWs growth rate, R_{axial}, is related to the T_f by the relation (*Klein et al. 2005*) as:

$$R_{axial} \propto \exp\left(\frac{-E_A^{Si}}{k_B T_f}\right) \tag{5.3}$$

where k_B is the Boltzmann's constant and E_A^{Si} is the activation energy for the catalytical decomposition of SiH_4 at heated tungsten filament (~2.43 eV) (*Van Veenendaal and Schropp 2002*). In order to confirm this relation, the variation of R_{axial} obtained from the experimental data and the fitted data from the above relation with T_f were plotted as shown in the Figure 5.9. A quite consistent result is observed between both data.

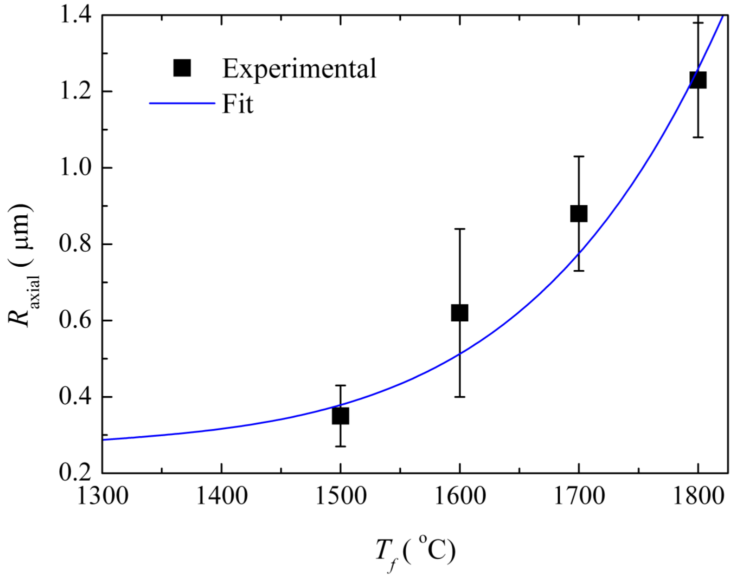

Figure 5.9: The variation of SiNWs growth rate, R_{axial} calculated from the experimental data and fitted by using the R_{axial} relation mentioned in the text with the T_f.

5.3.2 Energy dispersion X-ray linescan analysis and growth models

Deposition at T_f of ≤ 1400°C leads to the formation of larger size conical structures with the same shape as the In catalyst. An EDX line scan performed through the width of the conical structures [indicated by the arrow] is illustrated in FESEM image in Figure 5.10 (b). Only Si, O and In elements were detected inside the conical structures. The EDX line scan results show that higher intensity of Si element in the outer layer, while most of the In element was detected in the inner core of the conical structures. Meanwhile, the O content was constant within the conical structures. This indicates that the deposited Si tends to form a Si layer on the surface of In droplets, thus forming In-Si core-shell structure at $T_f \leq 1400^{o}$C, instead of inducing the growth of NWs. At T_f of $\geq 1500^{o}$C [Figure 5.10 (c)], the Si based radicals from SiH_4 form Si saturated In/Si alloy droplets inducing the growth of SiNWs from it. The SiH_x radicals dissolved into the molten In droplets, condense at the In/Si interface resulting in the crystal growth of SiNWs.

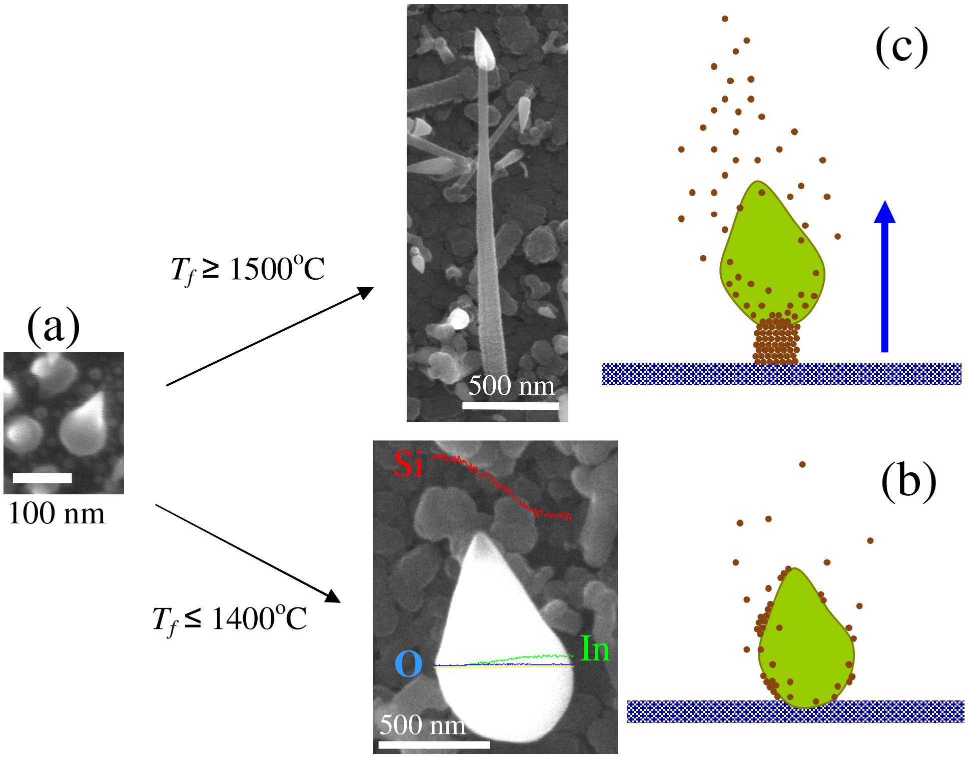

Figure 5.10: FESEM of the (a) In droplets, (b) typical conical structures present in samples prepared at T_f of 1300 and 1400^{o}C, and (c) typical In-catalyzed SiNWs grown at T_f of 1500^{o}C and above. Spectra inserted in (b) is the EDX line scan of the conical structures. The growth mechanism of the (b) In/Si core-shell conical structures and (c) In-catalyzed SiNWs are illustrated on the right hand side of the FESEM images.

5.3.3 X-ray diffraction

The structural properties of the samples were studied using XRD. The XRD patterns for

SiNWs synthesized at different T_f are depicted in Figure 5.11. The Si, In and In_2O_3 diffraction peaks are well indexed in the figure. An increase in T_f leads to several changes in the XRD patterns. The Si(111) peak is stronger and narrower in width for the samples prepared at higher T_f. The other Si diffraction peaks corresponding to the (220), (311) (400) and (331) crystallographic planes only appear in the sample deposited at $T_f \geq 1500^{o}C$. The highest intensity for the Si(111) peak indicates a preference of the (111) orientation along this crystallographic plane. At a lower T_f of 1300 to 1500°C, the $In_2O_3(222)$ diffraction plane made its appearance at $2\theta = 30.2\ ^{o}$, but is gradually suppressed with an increase in T_f. However, the In diffraction peaks with a preferred orientation along the (101) crystal plane existed in all the XRD patterns of the samples prepared at different T_f. The crystalline In_2O_3 layer is mostly formed at $T_f < 1500^{o}C$ and this produced a shielding on the surface of In catalyst. At higher T_f, the In_2O_3 layer is suppressed and the In catalyst is then exposed to activate the growth of the SiNWs, which remained as a capping droplet on the tips of the NWs. The In diffraction peaks in the XRD patterns are produced by this element present on the tips of the NWs. The absence of the $In_2O_3(222)$ diffraction peak in the samples deposited at higher T_f shows that the high crystallinity of the In caps of these NWs prevents post oxidation of the In capping droplets.

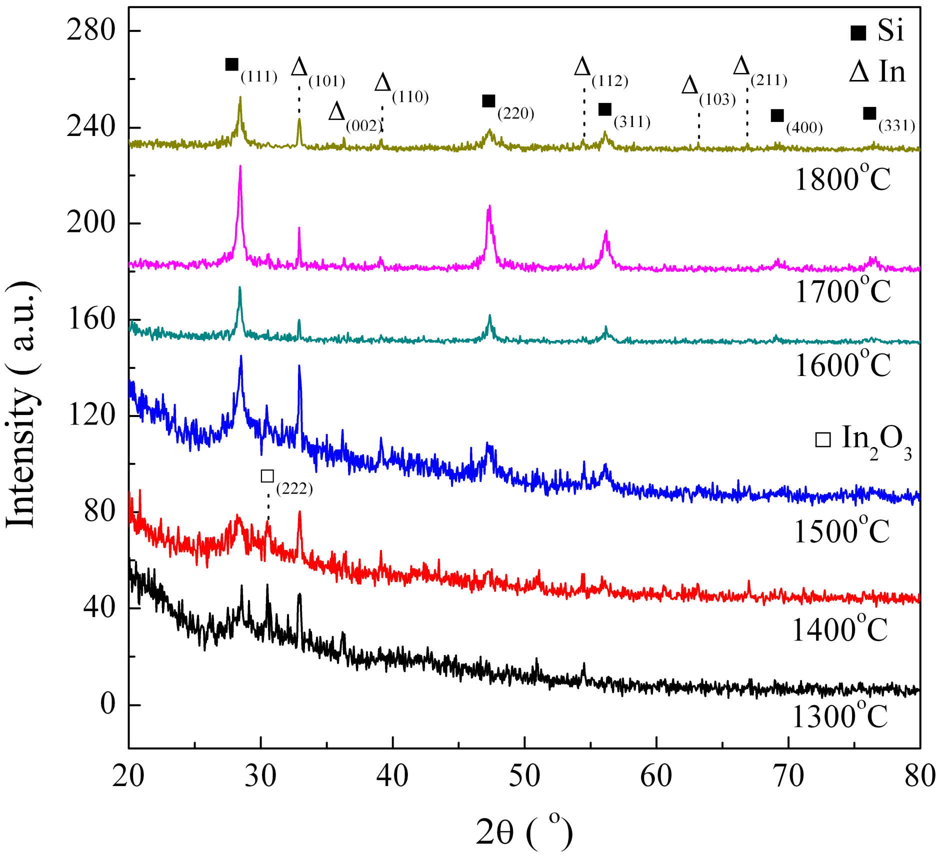

Figure 5.11: XRD spectra of the samples synthesized at different T_f. The crystal planes corresponding to Si, In and In_2O_3 crystal peaks were indexed according to the JCP2:00-026-1481, JCP2:01-085-1409 and JCP2.2CA:00-006-0416, respectively.

5.3.3 a) Analysis on FWHM of Si(111) diffraction peak

Further investigations on the influence of T_f on the crystalline structures of the samples are performed by deconvoluting the Si(111) diffraction peak using Lorentzian function fitting. The FWHM of the Si(111) diffraction peak at different T_f is plotted in Figure 5.12. The FWHMs for Si(111) peak are higher at low T_f, while the values decrease with increase in T_f. The reduction in width of the XRD peak is due to the enhancement in crystallinity of the samples and is associated with increase in size of the Si crystallites (*Kaelble 1967*). The FWHM values of the Si(111) peak seem to be constant at ~0.3 ° for $T_f \leq 1600^{\circ}C$, which indicates a more ordered structure was formed at T_f of 1600°C and above.

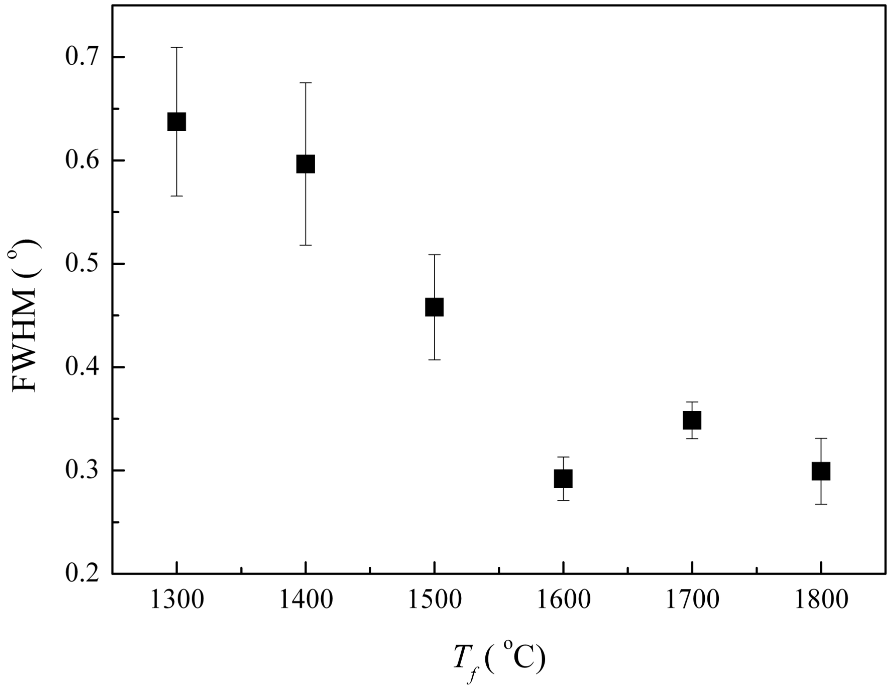

Figure 5.12: The variation of FWHM of Si(111) XRD peak with the T_f. The error bar represents the error of the fitting data.

5.3.4 Micro-Raman spectra

The crystallinity of the samples is further examined by Raman measurements. Figure 5.13 shows the Raman spectra of SiNWs synthesized at different T_f. The Raman peak located at wavenumber, ω~518 – 521 cm^{-1}, which corresponds to the TO-phonon mode of crystalline Si, is observed in all samples. An asymmetric broadening towards the lower frequency in the TO-phonon mode indicates a confined Si structure with grain boundary and amorphous phases, which is more significant at lower T_f. The Raman peak can be deconvoluted to two peaks at ~521 and ~500 cm^{-1}, which correspond to the crystalline and grain boundary components as shown in the inset of Figure 5.13.

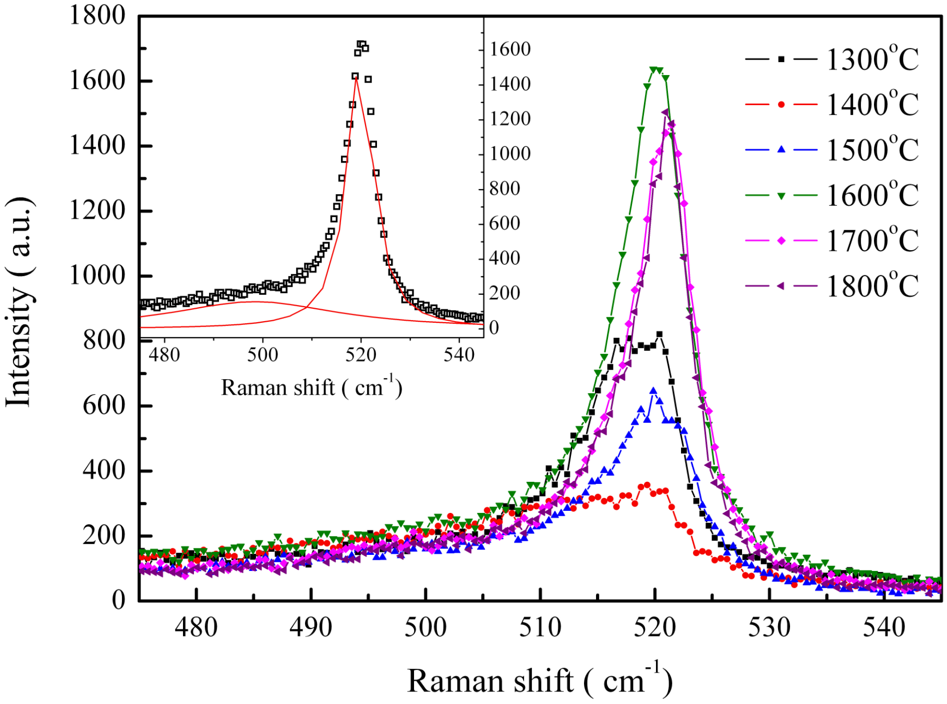

Figure 5.13: Raman spectra of the SiNWs synthesized at different T_f. The Inset is a typical Lorentzian fit of the TO-phonon mode of c-Si into crystalline (~520 cm^{-1}) and grain boundary (~500 cm^{-1}) components.

5.3.4 a) Analysis on Raman shift, FWHM and crystalline to grain boundary ratio

The shifting in the crystalline Si peak position from the single crystalline Si peak position (ω_o) is calculated as:

$$\Delta\omega = \omega_o - \omega \tag{5.4}$$

where ω_o = 521 cm^{-1}. The variation of the crystalline Si peak shifting, $\Delta\omega$, and the FWHM of the crystalline Si component of the samples with T_f are illustrated in Figure 5.14 (a). The result shows that $\Delta\omega$ is decreased with the increase in T_f. This represents an improvement in the formation of Si-Si bonds to form larger amount of crystalline lattices at higher T_f. The observed gradual decrease in FWHM of the crystalline Si peak from ~9.0 to 5.4 cm^{-1} with the increase in T_f is consistent with the observation from the XRD patterns of the samples. The reduction in FWHM of the crystalline Si peak is correlated to the improvement in crystalline quality to form less defect or defect-free structures (*Nguyen et al. 2009*). This agrees well with the XRD analysis as mentioned earlier. The lowest FWHM value of 5.4 cm^{-1} that is obtained is quite close to the measured FWHM of ~4.6 cm^{-1} for the single crystal Si. To attain a better understanding of the crystalline volume fraction of the samples, the ratio of the integrated intensity of crystalline to grain boundary components, I_C/I_{GB} with the T_f is plotted in Figure 5.14 (b). The ratio of the crystalline to grain boundary components is significantly increased at T_f of 1600°C and above. The XRD and Raman analysis obviously show that high T_f ($\leq$ 1600°C) induces the formation of crystalline structures in the NWs, which suppresses the grain boundary component from the samples.

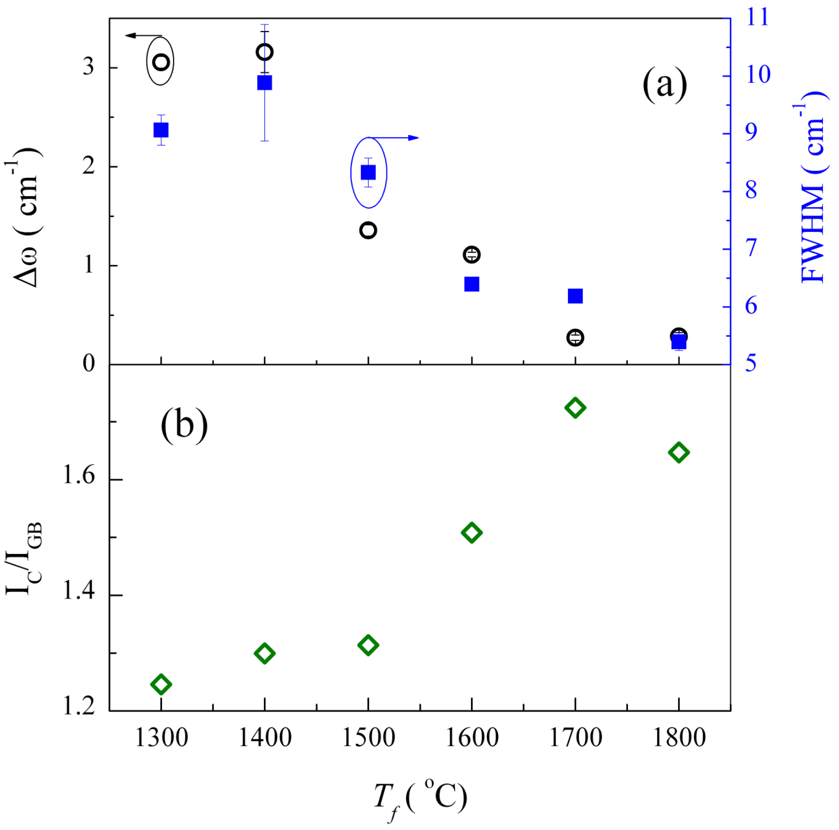

Figure 5.14: (a) The variation of crystalline Si peak shifting (Δω) and FWHM of TO phonon mode of crystal Si, and (b) ratio of crystalline to grain boundary components, I_C/I_{GB} with the T_f. The error bars represents the errors of the fitting data.

5.4 EFFECT OF DEPOSITION TIME ON GROWTH OF SILICON NANOWIRES

5.4.1 Growth of Si nanowires at different deposition times

5.4.1 a) Morphology

Figures 5.15 (a) – (c) present the FESEM images of the In-catalyzed SiNWs prepared at different deposition time, t_d of 5, 10 and 20 min. The morphologies of the NWs were highly dependent on the t_d. The SiNWs prepared at t_d of 5 min have large cone-shaped In catalyst capping the top of the NWs. The base diameters of the NWs range from 57 to 157 nm, while the NWs lengths vary from 0.6 to 1.9 µm. Some of the NWs show a kinked structure. The NWs were slightly tapered; however, the tapering effect is stronger for the longer NWs. An increase in t_d to 10 min resulted in the growth of needle-like SiNWs. The lengths of the NWs are more uniform and most of the NWs show a vertical inclination in one direction. The base diameters and lengths of the NWs increase to ~266 ± 13 nm and 2.9 ± 0.3 µm, respectively. Most of the In catalysts have migrated and formed sharp tips at the ends of the NWs. A further increase in t_d to 20 min only shows a small increase in length, but the diameter of the NWs is increased significantly. The base diameters and lengths of the NWs are around 496 ± 16 nm and 3.7 ± 0.2 µm, respectively. The sidewalls of the NWs become rough with morphology of interesting faceting radial growth structures.

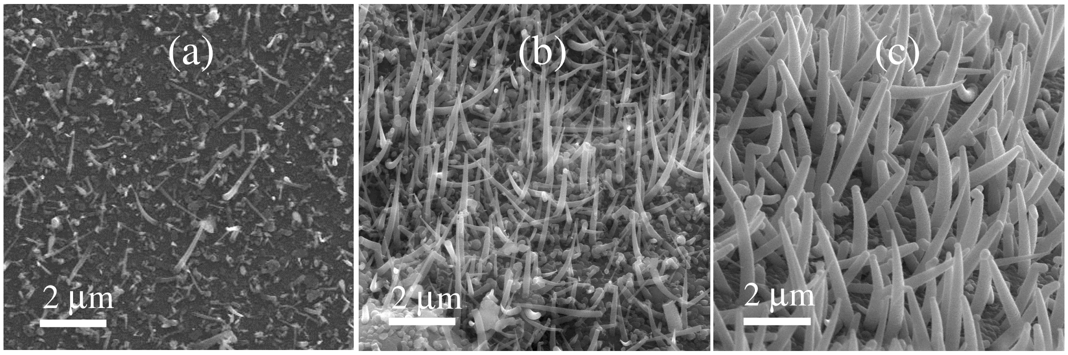

Figure 5.15: FESEM images of the In-catalyzed SiNWs synthesized at t_d of (a) 5 min, (b) 10 min, and (c) 20 min.

5.4.1 b) Variation of length, base radius of Si nanowires and In catalyst sizes with deposition time

The variation of l_{NW} and r_{base} of the SiNWs with t_{d} is plotted in Figure 5.16 (a). Both of l_{NW} and r_{base} increase with increase in t_{d}. However, the increasing rate of l_{NW} is reduced while the r_{base} is constantly increased with t_{d}. The R_{axial} calculated using the relation 2.1 are 0.26 ± 0.09 μm/min (t_{d} = 5 min), 0.28 ± 0.06 μm/min (t_{d} = 10 min) and 0.19 ± 0.02 μm/min (t_{d} = 20 min). The R_{axial} is about constant at t_{d} below 10 min, while it is reduced to half when t_{d} increased to 20 min. The decrease in R_{axial} when t_{d} is above 10 min is expected to be related to the migration of In catalyst. The variation of l_{NW} with the In catalyst sizes is plotted as shown in Figure 5.16 (b). A reduction in In catalyst size with increase in l_{NW} is observed. The size of In catalyst is decreased to half when the l_{NW} exceeds 2 μm, and it is rapidly decreased with further increases in l_{NW}. The rapid migration of In catalyst may influence the catalytic growth, resulting in the decrease in R_{axial} of SiNWs. The radius of the SiNWs increases constantly from t_{d} of 5 to 20 min as shown in Figure 5.16 (a). The linearity of the graph indicates that the growth rate of columnar Si is constant and is not affected by the In catalyst. The radial growth rate, R_{radial} calculated from the relation 2.3 is ~12 ± 0.1 nm/min. The core radius of the single crystalline SiNWs, r_{o}, is deduced by extrapolating the linear graph to the y-intercept.

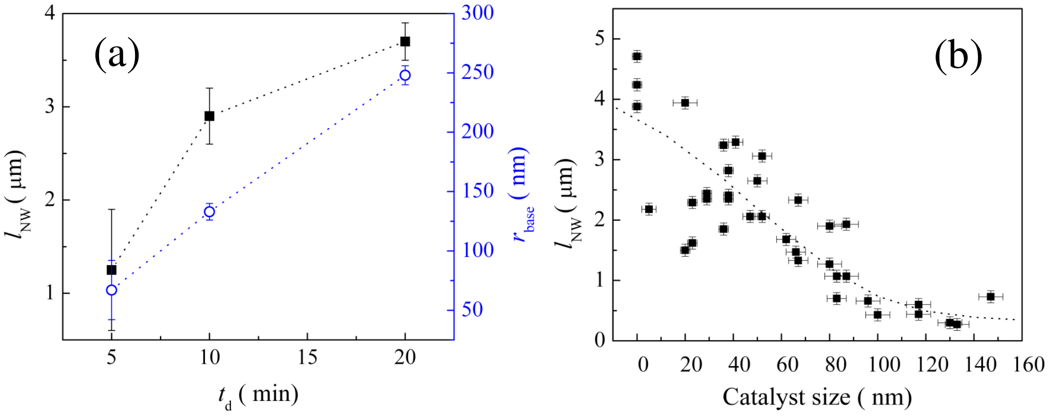

Figure 5.16: (a) The variation of l_{NW} and r_{base} of the In-catalyzed SiNWs with t_{d}, and (b) the variation of l_{NW} with the catalyst sizes.

5.4.2 Auger electron spectra

A typical Auger electron spectrum of the In-catalyzed SiNWs is illustrated in Figure 5.17 (a). With assistance of the electron microscope, the Auger signal on single SiNWs can be obtained by pointing the probe to the position of NWs from electron microscope image [inset in Figure 5.17 (a)]. Figure 5.17 (b) shows suppression in In MNN peak with increase in t_d. This indicates a decrease in In element in the samples with increase in t_d. This is consistently agreed with the observation from FESEM images. The ratio of In to Si concentration (In%/Si%) is decreased from 0.08 to 0.04 and 0.03 as the t_d is increased from 5 to 10 and 20 min, respectively.

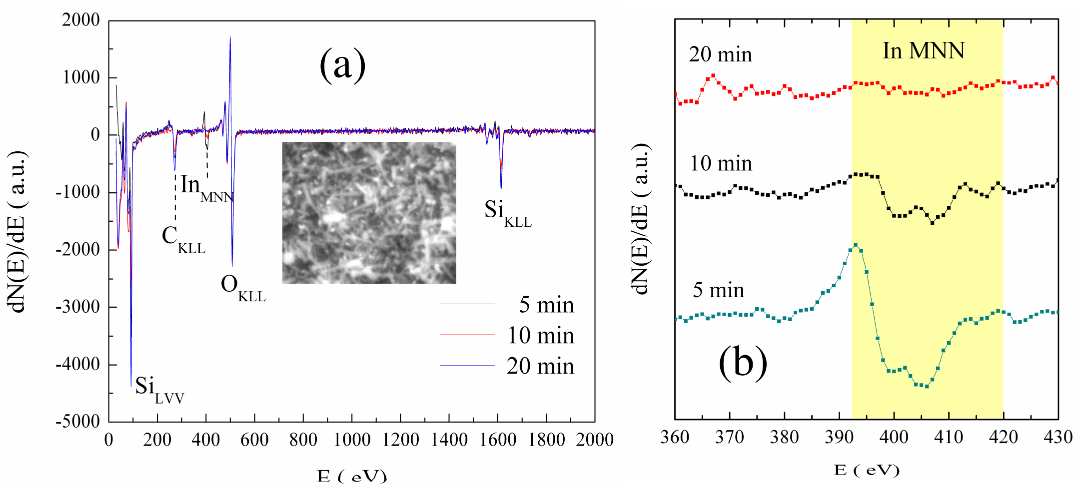

Figure 5.17: (a) typical Auger spectrum of the In-catalyzed SiNWs. (b) The variation in In MNN peak from Auger spectra with different t_d.

5.4.3 Structural properties – X-ray diffraction and Raman analysis

The structural properties of the In-catalyzed SiNWs are examined by XRD and Raman measurements as depicted in Figures 5.18 (a) and (b), respectively. Weak crystalline Si(111), In_2O_3(222), In(101), Si(220) and Si(311) diffraction peaks are observed in the XRD pattern of the In-catalyzed SiNWs sample prepared at t_d of 5 min. The In_2O_3(222) diffraction peak is suppressed when t_d is increased to 10 min, leaving only In(101) peak in the spectrum. The In-catalyzed capping the end of the NWs [Figure 5.15 (b)] contributes to the In(101) diffraction plane. The In diffraction peak is completely suppressed for the sample prepared at t_d of 20 min, which explains the absence of In catalyst cap in the SiNWs as shown by the FESEM images [Figure 5.15 (c)].

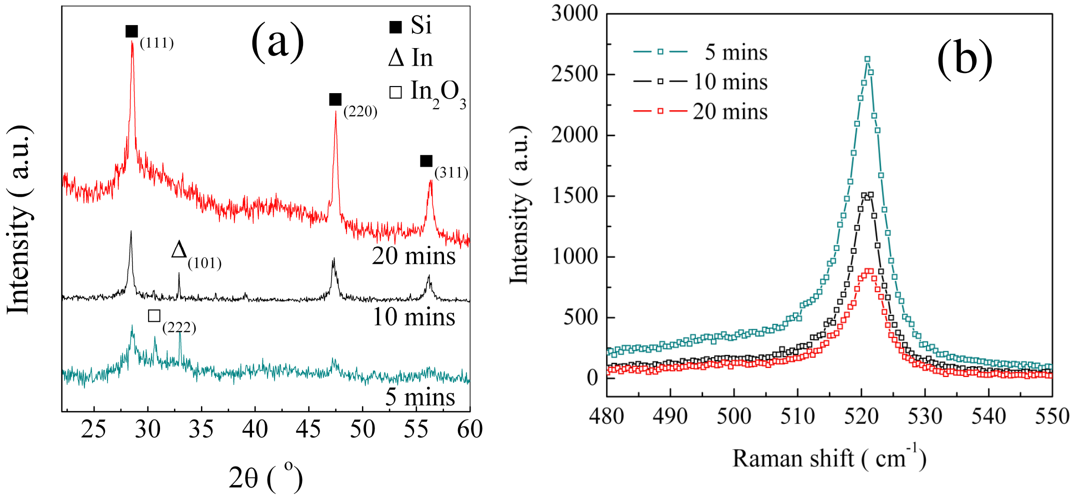

Figure 5.18: (a) XRD patterns and (b) Raman spectra of the In-catalyzed SiNWs synthesized at t_d of 5, 10 and 20 min. The crystal planes corresponding to Si, In and In_2O_3 crystal peaks were indexed according to the JCP2:00-026-1481, JCP2:01-085-1409 and JCP2.2CA:00-006-0416, respectively.

On the other hand, the crystalline Si diffraction peaks become sharper with higher intensity for the SiNWs synthesized at t_d of 10 min. This indicates an enhancement in crystallinity of sample. The increase in number density of the crystalline SiNWs grown at t_d of 10 min contributes to the increase in intensity indicating that the NWs are highly crystalline. From Raman spectrum, the TO-phonon mode of crystal Si (521 cm^{-1}) becomes more symmetric and the FWHM of the TO mode decreases from 6.0 ± 0.1 to 5.4 ± 0.1 cm^{-1} as the t_d increases from 5 to 10 min. This confirms the increase in crystallinity of samples as observed in XRD pattern.

Two observations are revealed in the XRD diffraction peaks of Si when the t_d is increased to 20 min. These are the presence of amorphous-like background and the broadening of Si peaks. The FWHM of the Si(111) peak is increased from 0.36 ± 0.01 to 0.41 ± 0.02^{o} .The peak broadening is always related to the reduction in crystallite size and formation of Si grains (*Kaelble 1967*). Similarly, Raman spectrum reveals an asymmetric broadening of the TO-phonon mode and shifting of this peak towards lower frequency. The FWHM of TO mode increases from 5.4 ± 0.1 to 6.6 ± 0.1 cm^{-1} at t_d of 20 min. The shifting of the TO-phonon mode from the Brillouin zone is due to the dislocation of the crystalline structure and the formation of crystal Si grains (*Gouadec and Colomban 2007*). Since the SiNWs are single crystalline in structure, the formation of crystal Si grains is believed to originate from the radial growth Si structures.

5.4.4 High resolution transmission electron microscopy

The TEM micrograph of the needle-like tapering SiNWs synthesized at t_d of 10 min is shown in Figure 5.19 (a). The morphologies of the NWs and the faceting structures on the sidewalls of the body and root of the NWs are observed from the TEM micrograph. A SAED pattern taken from the near end of the NWs, as shown in Figure 5.19 (b), suggests that the NWs are single crystalline with cubic Si structure. The discrete diffraction spots corresponding to the Si[-111] zone axis are indexed in the SAED pattern. The HRTEM image taken on the tip of the NWs [Figure 5.19 (c)] reveals that an In droplet capped on the tip of the NWs. The size of the In catalyst is relatively smaller than the initial size of the In catalyst (67 ± 20 nm). The lattice spacings measured from these images are 0.27 and 0.31 nm, which correspond to the lattice spacings for In(101) and Si(111) orientations planes, respectively. The HRTEM image scanned on the sidewall of the NWs [Figure 5.19 (d)] reveals the single crystalline structures of the SiNWs. The sidewall of the SiNWs is covered by a thin layer (2 – 3 nm) of SiO_x. Detailed analysis done on the crystalline lattices of the SiNWs shows an incorporation of In within the matrix of the SiNWs as illustrated in Figure 5.19 (e). It is believed that the In element originated from the In catalyst, which has migrated to the sidewalls of the NWs during the axial growth process. The migration of these In atoms may form clusters in a molten form, which is easily bonded to the dangling bonds of Si on the sidewalls of the NWs. However, the EDX analysis (Figure 5.2) showed no trace of other elements besides the Si and O elements on these NWs. This indicates that from the detection limits of EDX, less than 1% of In element is confirmed to be present in the SiNWs. From the TEM image, it is observed that high density radial growth of Si structures is uniformly distributed along the walls of the body and base of the NWs. The magnified TEM image of these radial growth Si structures in Figure 5.19 (f) shows a large area of nanocolumnar Si structures covering the sidewall of the NWs. These nanocolumnar structures are slanted at an angle of approximately 68^{o} towards the walls of the NWs. The diameters of the nanocolumnar Si structures vary from 12 to 25 nm with an average diameter of ~18 ± 3 nm. Figure 5.19 (g) presents the HRTEM micrograph of the nanocolumnar structures. A mixed phase of several to tens of nanometers of crystalline Si structures, embedded in between amorphous Si grain boundary is observed within the nanocolumnar structures. This indicates that the Si nanocolumns are nanocrystalline (nc) in structure.

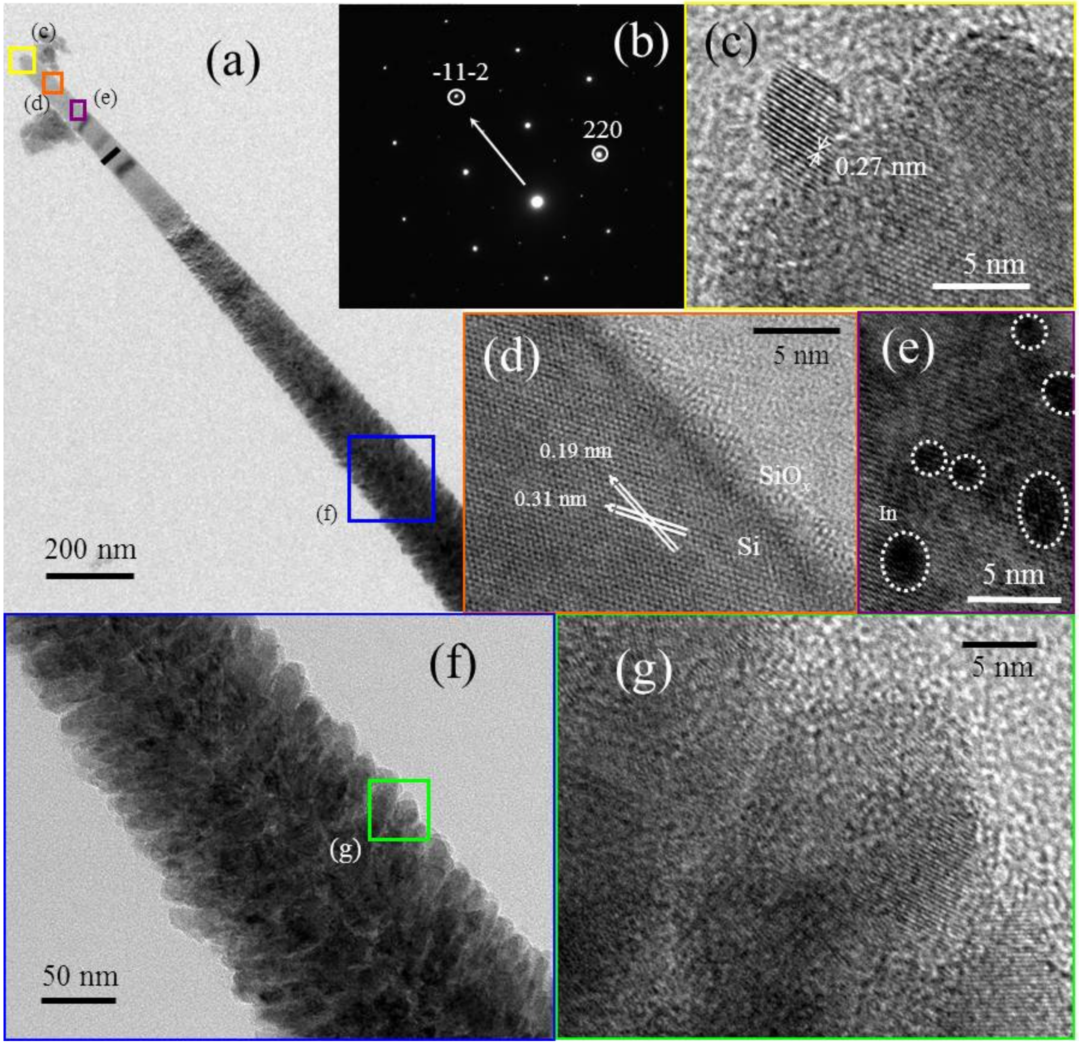

Figure 5.19: (a) typical TEM image of the In-catalyzed SiNWs synthesized at t_d of 10 min. (b) SAED pattern of the NWs taken at [-111] zone axis. The HRTEM images of the (c) tip, (d) near end sidewall, (e) body, and (f) near base of the NWs magnified from the TEM image. The HRTEM image of the (g) columnar structure magnified from (f).

5.5 GROWTH MECHANISMS

5.5.1 Axial growth process of In-catalyzed Si nanowires

Figure 5.20 illustrates the FESEM images of the as-grown In-catalyzed SiNWs synthesized by HWCVD at different growth stages. From the growth process, a proposed growth mechanism for the In-catalyzed SiNWs using HWCVD is presented.

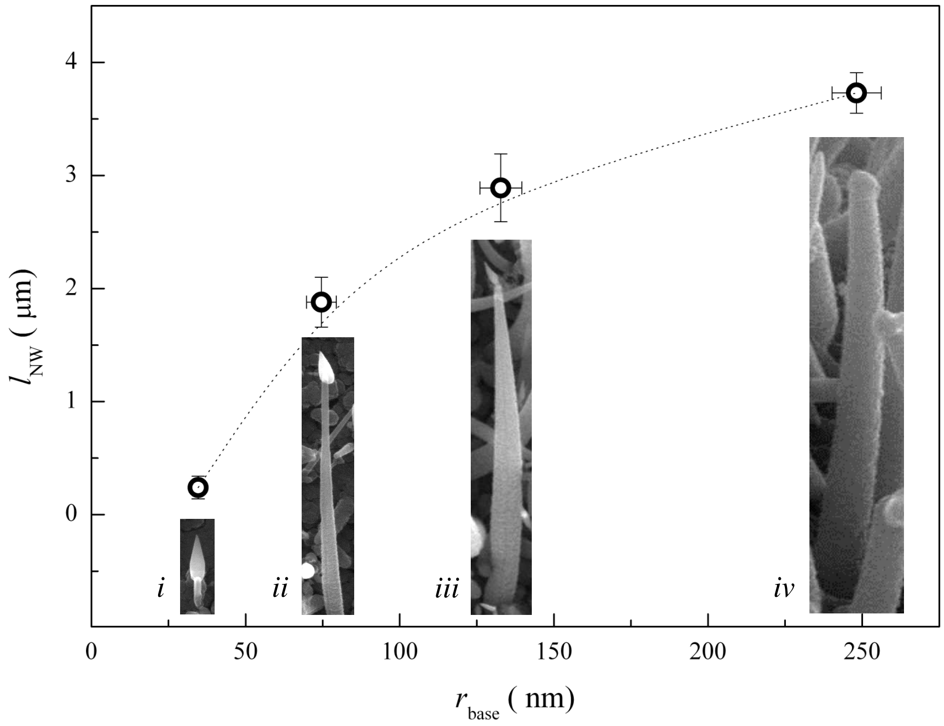

Figure 5.20: FESEM images at different growth stages of the In-catalyzed SiNWs synthesized using HWCVD, and (Graph) variation of l_{NW} with r_{base} at each growth as illustrated by FESEM images.

The axial growth process of the NWs as reported by a number of researchers generally follows the VLS growth mechanism (*Givargizov 1975; Kolasinski 2006; Schmid et al. 2008*). As mentioned before, the evaporated In catalyst initially forms cone-shaped structure as a results of the H_2 plasma treatment during the evaporation process. The molten In catalyst forms a large contact angle of approximately 125 ^{o} with the Si substrate, while the vertical cone shape of the In catalyst reduces the area of In/Si interface. This initiated the growth of a smaller diameter of SiNWs, capped with a large cone shaped In catalyst droplet. A large quantity of silyl and other radicals including Si, SiH_3, Si_2H_x (x = 2, 4 and 6), which are thermally decomposed from SiH_4 by the HW filament are diffused into the cone-shaped In catalyst on the substrate and forms In-Si eutectic composites. The continuous diffusion of those reactive radicals into the In catalyst results in the self-arrangement and precipitation of Si adatoms at the In/Si interface to form epitaxial growth of the single crystalline SiNWs. In the early stage of the growth process, the NWs formed are straight and uniform in diameter, as shown in Figure 5.20 (*i*). During the axial growth process, the uncatalyzed reactive SiH_x radicals surrounding the sidewalls of NWs are absorbed onto the surface of the NWs. This produces the radial growth of the NWs thus forming the tapering NWs as illustrated in Figures 5.20 (*ii*) and (*iii*). The size of the In catalyst cap decreased to a point where the NWs with catalyst caps no longer exist during the growth process of the SiNWs [Figures 5.20 (*i*) – (*iv*)].

5.5.2 Indium catalyst kinetics

From FESEM and Auger analysis, the size of In catalyst droplets is reduced and eventually disappears with increase in t_d, which indicates a migration of catalyst in conjunction with the axial growth of SiNWs. This interesting phenomenon has been discussed in previous studies to explain the dynamics of the catalyst (*Kodambaka et al. 2006; Madras et al. 2010*). Hannon et al. (*Hannon et al. 2006*) suggested the migration of the catalyst to neighboring catalysts and to the sidewalls of the NWs. Meanwhile, Spanier et al. (*Cao et al. 2006*) suggested two possible pathways for the catalyst transfer, which are through liquid-solid (L-S) and vapour-liquid (V-S) interfaces during the VLS process. Kolasinski (*Kolasinski 2006*), in an investigation of the VLS growth process, mentioned that the change of catalyst radius with respect to time, $dr/dt < 0$, led to the termination of the growth of the NWs. In parallel to these previous literatures, the size reduction of the In catalyst is attributed to the evaporation of the In catalyst. The probability of In diffusing into the Si matrix through the In/Si interface is known to be low due to the low diffusivity of In into Si. Only the In catalyst at the surface can gain sufficient energy from the SiH_x reactive radicals before being able to diffuse into the Si matrix. These In atoms with higher energy eventually evaporate and wet the sidewalls of the NWs, resulting in the reduction of the size of the In catalyst at the tip, while retaining the shape. The more energetic In atoms would then be trapped by the NWs sidewalls and incorporated into the SiNWs networks or extracted out from the reactor through pumping. The electronic structure of In makes it a natural acceptor of electrons when bonded to Si atoms, therefore the In diffusion into the Si networks results in a p-type doping in the SiNWs. Furthermore, it is interesting to note that the growth of NWs is slowed down and terminated when the In droplets reach a critical size, d_c. At this d_c, the diffusion of SiH_x radicals into the catalyst could no longer induce precipitation of Si atoms, and therefore terminate the axial growth. The fundamental details on the Si nuclei formation in the liquid catalyst have been reported by Sharma et al. (*Sharma et al. 2005a*) and Tan et al. (*Tan et al. 2004*). The In catalyst continues to evaporate, leaving a pit of a size equivalent to the d_c on top of NWs.

5.5.3 Growth process of slanting-Si nanocolumns on Si nanowires

A typical TEM image of the SiNWs is illustrated in Figure 5.21 (a). Radial growth of columnar structures is observed in the body of the NWs and which is believed to contribute to the tapering of NWs. The diameter of the columnar structures is approximately 18 ± 3 nm. The radial growth of columnar Si structures is also evidenced in the TEM image of the sidewalls of the SiNWs.

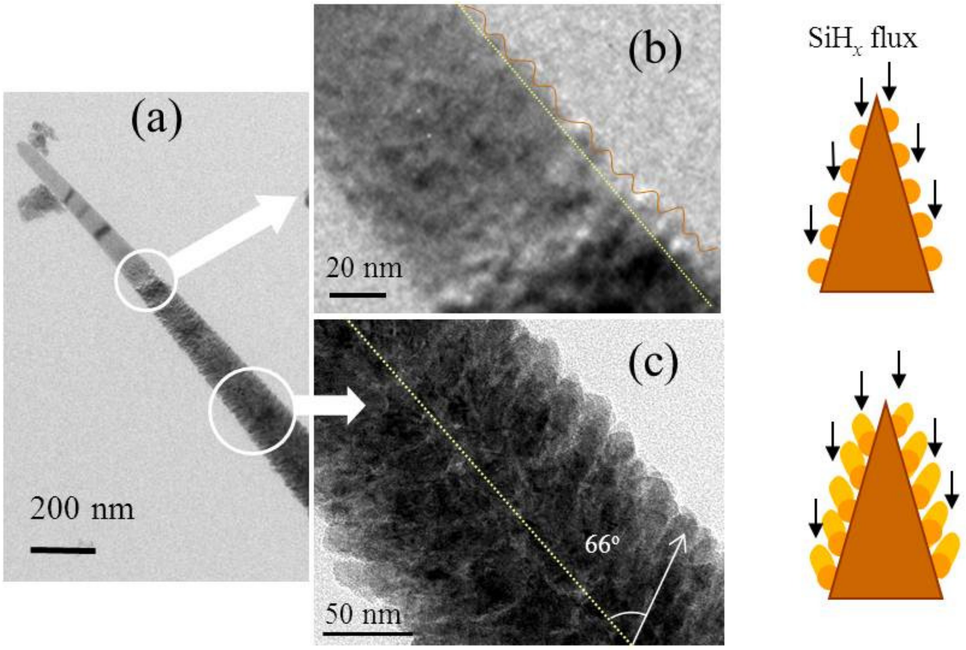

Figure 5.21: (a) TEM image of In-catalyzed SiNW, and magnified TEM images of the (b) initial growth stage of the radial growth structures, and the (c) radial growth slanting-columnar structures. The mechanism of the radial growth process is presented on the right hand side of the figure.

Contrary to the VLS axial growth mechanism, the growth process of the Si nanocolumns is due to the VS growth mechanism, which is usually applied in the two-dimensional thin film growth model (*Amanatides and Mataras 2011*). In the initial stages of the growth process, reactive SiH_4 radicals are adsorbed onto the surface of the NWs to form several monolayers of Si film. The nucleation and coalescence of the Si layer leads to the formation of islands on the walls of the NWs (*Kołodziej 2004*), as shown in Figure 5.21 (b). As the NWs grow, the walls of the NWs receive an incident flux of SiH_4 radicals at a specific angle from the deposition source. The nucleated islands shield the other sides of the film from growth (*Liu et al. 2009; Zhao et al. 2003*). Most of the SiH_4 radicals diffuse into the Si islands, resulting in the growth of slanting-columnar structures, as shown in Figure 5.21 (c). Si nanocolumns are slanted at an angle of ~66 ° toward the sidewalls of the NWs. Further investigation of the TEM micrographs reveals that the slanting angle of Si nanocolumns from the sidewall of the NW ranges from 38 to 70 ° [Figure 5.22 (a) – (d)].

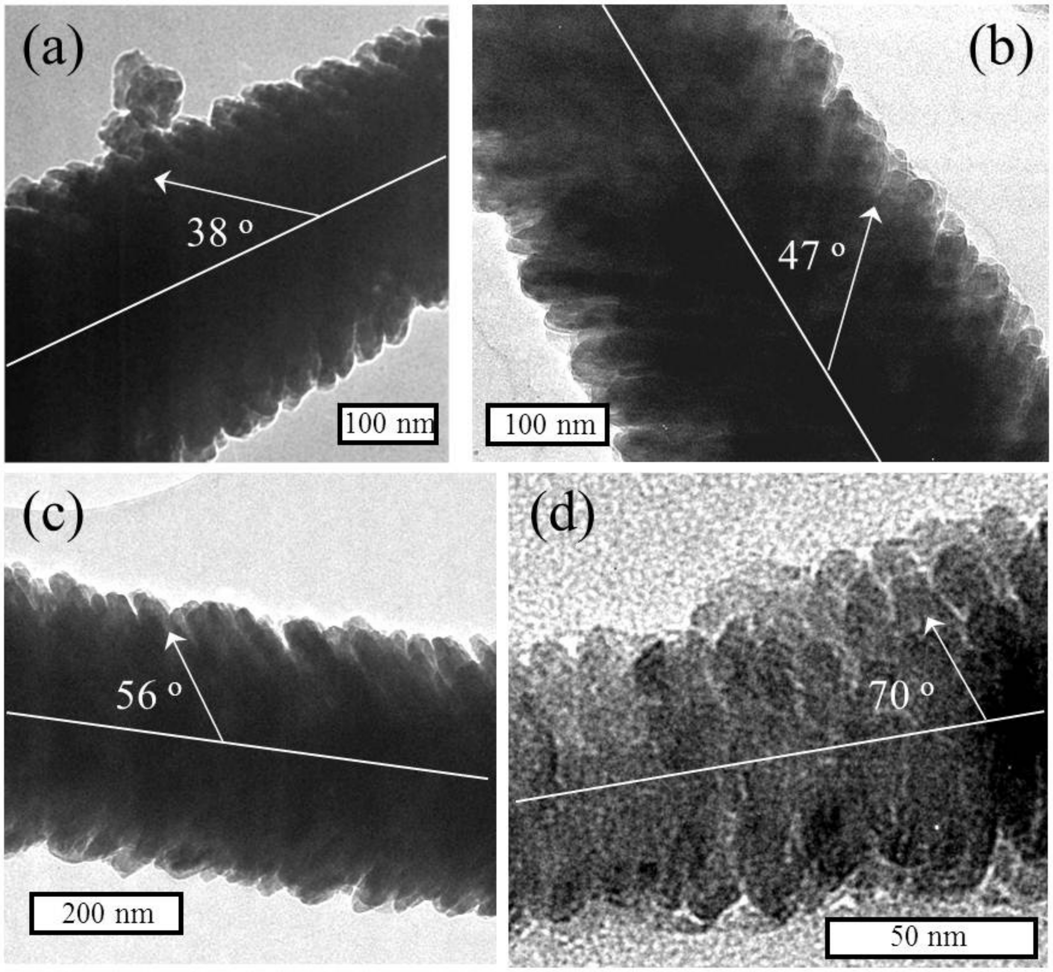

Figure 5.22: TEM micrographs of the SiNWs with different slanting angles of Si nanocolumns of (a) 38 ^{o}, (b) 47 ^{o}, (c) 56 ^{o} and (d) 70 ^{o} clad on the NWs' sidewalls.

5.5.4 Formation of crystalline Si/slanting Si nanocolumns core-shell nanowires

From the previous discussion, the axial growth of NWs is dependent on the catalyst. During axial growth, the In catalyst evaporates and condenses on the sidewalls of the NW (*Hannon et al. 2006; Madras et al. 2010*) or becomes incorporated into the SiNW through diffusion (*Cao et al. 2006; Yu et al. 2011*). As a result, the size of the catalyst gradually decreases, leading to the cessation of axial growth. Increase in t_d terminates the axial growth, making the radial growth of uncatalyzed Si more dominant in the deposition. TEM micrographs in Figure 5.23 (a) – (c) present the growth process of the

Si nanocolumns on the surface of the SiNWs. From Figure 5.23 (b), it can be seen that when the axial growth process of SiNWs is terminated, the excess of SiH_x radicals mainly contribute to radial growth. The diameter of NWs increases significantly with further increase in t_d. As a result, the surface of the NWs is surrounded by a high density of slanting-columnar Si structures [Figure 5.23 (c)], which form a single crystalline Si core and slanting Si nanocolumns cladding NWs.

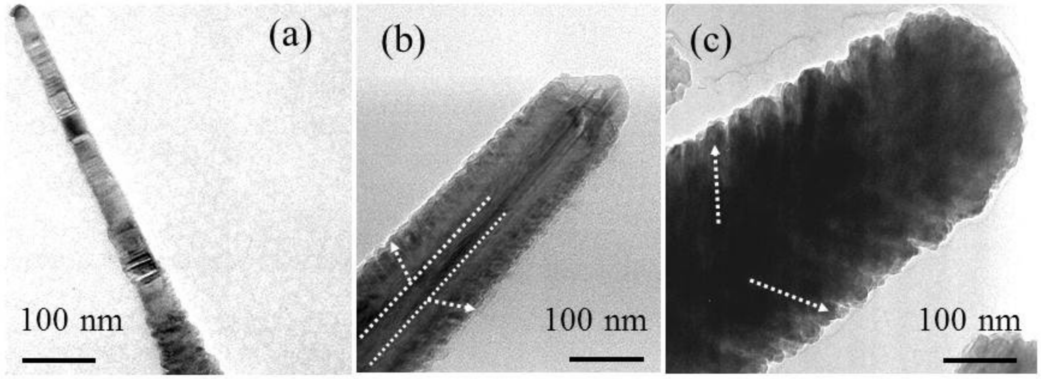

Figure 5.23: (a) axially grown In-catalyzed SiNWs, (b) and (c) radially grown slanting Si nanocolumns on the surface of the NWs.

5.5.5 Growth model of crystalline Si/slanting Si nanocolumns core-shell NWs

From these results, a growth model on the formation of the crystalline Si/slanting Si nanocolumns core-shell NWs is proposed and is illustrated in Figure 5.24, to conclude the growth mechanism of the In-catalyzed SiNWs using HWCVD technique. During the axial growth of SiNWs from the In catalyst, uncatalyzed SiH_x radicals are incorporated into the NW network through a VS growth process. Similar to oblique angle deposition reported by Zhao et al. (*Zhao et al. 2003*), the islands shield other areas from growth and form columnar structures with a tilted geometry. The Si nanocolumns tilt angle with respect to direction of incident SiH_x radical flux, β, is related to the oblique angle of NW with the incident flux, α, as (*Tait et al. 1993; Ye et al. 2004*):

$$\tan\beta = \frac{1}{2}\tan\alpha \tag{5.5}$$

for α between 0 to 60 ^{o}, and

$$\beta = \alpha - \sin^{-1}\left[\frac{(1-\cos\alpha)}{2}\right] \tag{5.6}$$

for larger α.

The inclination angle of the NWs, θ_{NW} is geometrically equal to the θ, as the:

$90-\theta_{NW} = 90-\alpha$, hence, $\theta_{NW} = \alpha$.

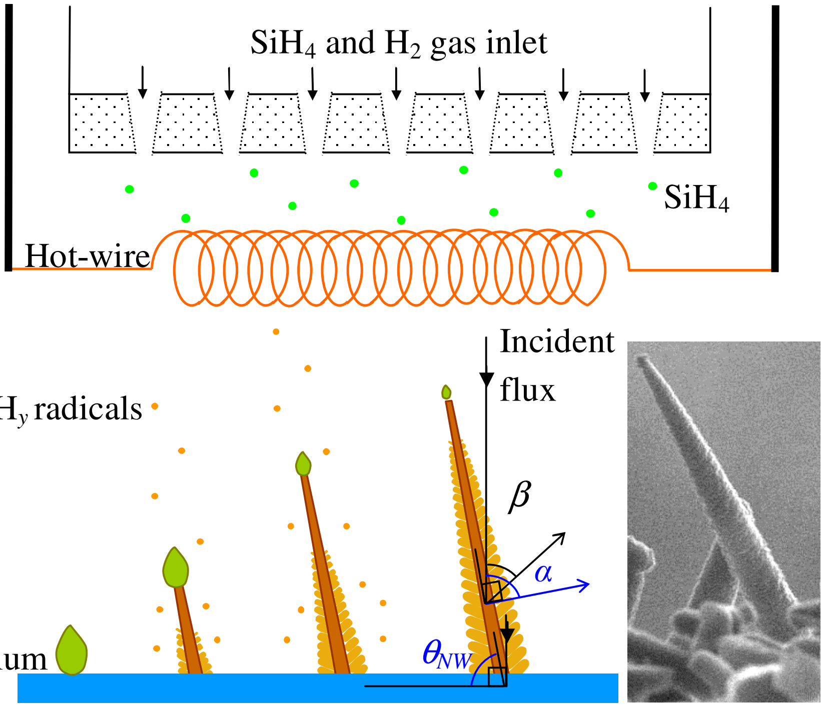

Figure 5.24: The proposed axial and radial growth mechanism of the crystalline Si/slanting Si nanocolumns core-shell NWs synthesized by HWCVD.

5.6 SUMMARY

SiNWs were successfully synthesized by using In catalyst and HWCVD technique. High purity of Si and good crystalline structures of SiNWs were obtained in this study. Decrease in In droplets size increases the axial growth rate, decreases the tapering parameter and results in better alignment of NWs. The threshold T_f for the growth of the straight and tapered SiNWs is 1500°C. This is consistent with the initial temperature for the desorption of the Si radicals from the HW surface. It showed that the growth rate, number density and crystallinity of the SiNWs can be enhanced by increasing the T_f. Meanwhile, the growth mechanism of the In-catalyzed SiNWs using HWCVD technique was studied. A number of observations on this low temperature CVD processing growth of the In-catalyzed SiNWs, such as the axial growth mechanism, the catalyst kinetics during the growth process and the radial growth of the slanting Si nanocolumns were discussed in the chapter. The radial growth of columnar nc-Si structures and axial growth of NWs resulted in the formation of a novel core-shell NW structure. These columnar structures displayed a growth rate of ~12 ± 0.1 nm/min.